applied optics

OPSR enhancement of high-temperature operating shallow-surface grating VCSELs

Yingying Liu,[1,2] Xing Zhang,[1,*] Youwen Huang,[1,2] Jianwei Zhang,[1] Werner Hofmann,[3] Yongqiang Ning,[1] and Lijun Wang[1]

[1]State Key Laboratory of Luminescence and Applications, Changchun Institute of Optics, Fine Mechanics and Physics, Chinese Academy of Sciences, Changchun 130033, China
[2]University of Chinese Academy of Sciences, Beijing 100049, China
[3]School of Solid State Physics, Technical University of Berlin, Berlin 10623, Germany
*Corresponding author: zhangx@ciomp.ac.cn

Received 2 February 2018; revised 2 May 2018; accepted 2 May 2018; posted 3 May 2018 (Doc. ID 321380); published 25 May 2018

A polarization-stable single-mode 894 nm vertical cavity surface emitting laser (VCSEL) with an orthogonal polarization suppression ratio of 30 dB, even at a temperature up to 80°C, was achieved for atomic clock applications by utilizing shallow-surface gratings. An improved grating VCSEL fabrication technology for mass production was also proposed by taking advantage of the displacement Talbot lithography. The multi-mode grating VCSEL was also measured for other applications that need polarization stability, such as doubled-data-rate polarization multiplexed free-space links.

OCIS codes: (140.7260) Vertical cavity surface emitting lasers; (140.5960) Semiconductor lasers; (050.2770) Gratings; (240.5440) Polarization-selective devices.

https://doi.org/10.1364/AO.57.004486

1. INTRODUCTION

Vertical cavity surface emitting lasers (VCSELs) offer numerous advantages, such as low power consumption, high modulation bandwidth, and favorable beam characteristics. These properties make them suitable for many applications, such as optical storage, laser printing, spectroscopy, and miniature atomic clocks. However, not only single transverse mode operation but also polarization stability is indispensable for the above-mentioned applications. In VCSELs, the two polarizations degenerate due to their isotropic gain, the cylindrical resonator, and mirrors with a polarization independent reflectivity [1]. VCSELs, however, grown on conventional (100)-oriented GaAs or InP substrates possess a preferred polarization of the individual modes along the [011] and [0–11] crystal axes. This is caused by the electrooptic effect that is induced by the doping in the Bragg mirrors [2]. The first higher transverse mode is polarized orthogonal to the fundamental mode in most cases, and further higher-order modes may assume either of two polarizations. No general polarization selection rule is identified. When the driving current or the operating temperature changes and the strain or an optical feedback is applied, the polarization of every individual mode can abruptly change from one preferred crystal axis to the other. This phenomenon is called polarization switching [3].

To overcome this drawback, many attempts have been undertaken that can be roughly divided into two main types of action: anisotropic gain or polarization-dependent resonators. Anisotropic gain can be achieved by growth on GaAs (311) B substrates with high crystal indices [4]. However, this method results in challenging crystal growth and cannot monolithically integrate two VCSELs with orthogonal polarization on one chip. Anisotropic gain can also be realized by asymmetric current injection [5] or by changing strain [6]. A second possible approach is polarization-dependent loss in the resonator by integrating mirrors with a polarization-dependent reflectivity. Dumbbell- [7] or elliptically [8] shaped mesas have also been used. However, the noncircular geometries lead to noncircular far field and awkwardly control the polarization of multimode VCSELs. Metal and metal-semiconductor surface gratings have also been investigated, but they are found to be a weak polarization control [9]. Pure semiconductor surface gratings have been successfully realized [10–12] and found to provide a stronger polarization control than a metal or a metal-semiconductor grating [13]. The best performance taking advantage of this method is 40 dB of peak-to-peak difference between the dominant and suppressed polarization modes called peak-to-peak orthogonal polarization suppression ratio (OPSR) [14]. High-contrast grating (HCG) instead of part of a high-reflectivity top mirror [15–17] incorporated into the VCSEL structure is a new method to control the polarization state. A peak-to-peak OPSR of 36 dB has been achieved by utilizing a HCG [18]. A single polarization VCSEL hybridly

Table 1. Comparison of Different Grating Fabrication Technologies

Grating Type	HCG	Subwavelength Grating	Surface Grating
Fabrication technology	Electron beam lithography	Nanoimprint lithography	Displacement Talbot lithography
Achievable limits	Nanoscale	Nanoscale	Nanoscale
Advantages and disadvantages	Difficult to achieve high-precision process requirements	High-temperature fabrication problem	Time saving, low cost, mass production

integrated with silicon gratings [19] has been reported recently. However, these methods of grating fabrication mentioned above are costly and require a time-consuming electron beam lithography technology. Nano-imprint lithography (NIL) as an alternative was proposed [20,21], whereas this method requires high-temperature fabrication, which results in dimensional errors and mold release difficulties during pattern transfer. Moreover, particulate contamination and the residual polymer layer are remaining difficulties. The grating defined by displacement Talbot lithography (DTL) [22,23] was a mask-based photolithography technique for patterning high-resolution periodic patterns. The accuracy could also achieve the nanometer level as electron beam lithography. The method is time saving, low cost, and suitable for mass production. Table 1 shows the comparison of different grating fabrication technologies.

In this study, a type of polarization-stable single-mode 894 nm VCSEL is fabricated with shallow-surface grating, which may be applied for atomic clocks. The process of grating fabrication is especially improved. The method for the particular VCSEL is as simple as possible to a standard one and is low cost to be suitable for mass production, taking advantage of DTL. Moreover, a two-exposure technology was added to make the DTL adapt to the production process of VCSEL. Numerical calculations of the polarization-dependent modal loss were also performed to provide information on the required precision in the fabrication of an optimized design. The multimode grating VCSEL was also measured for other applications that need polarization stability, such as doubled-data-rate polarization multiplexed free-space links.

2. OPTIMIZED SURFACE GRATING VCSEL DESIGN

To optimize the polarization control properties of the grating VCSEL, we calculated the threshold gain of different polarization orientations and relative dichroism (RD) with a large range of grating depths. The coupled wave method is applied for analyzing electromagnetic wave diffraction by grating [24]. Its theoretical formulation, which does not require sophisticated numerical techniques, is suitable for gratings that possess continuous permittivity variations (volume gratings) or discontinuous permittivity variations (surface-relief gratings). When integrating a surface grating into a VCSEL, the two main polarizations experience different reflectivity of the upper mirror and therefore different threshold gains of two polarizations. The longitudinal position of the standing wave, especially on the depth of the grating, is displayed in the graph of Fig. 1(a). The model exhibits that the variations in the grating depth can lead to different polarization orientations. In Fig. 1(b), the calculated RD resulting from these different threshold gains is given. The RD is simply defined as

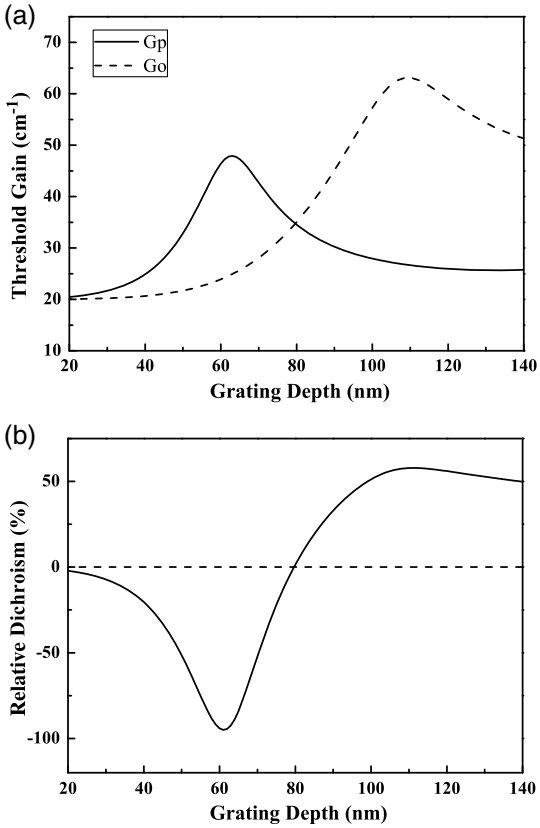

Fig. 1. (a) Calculated threshold gains for the polarization parallel (G_p) and orthogonal (G_o) to the grating grooves. (b) Relative dichroism calculated from the threshold gains.

$$\mathrm{RD} = 1 - \frac{G_p}{G_o}, \tag{1}$$

where G_p and G_o denote the threshold gain of the polarization parallel and orthogonal to the grating grooves, respectively. Therefore, a negative RD when $G_p > G_o$ indicates a prior polarization orthogonal to the grating grooves, and vice versa. The simulations predict a strong dichroism peak observed around a grating thickness of 60 nm. The simulation is conducted for the fundamental mode with a duty cycle (the ratio of ridge width to period) of 50% and a grating period of 600 nm.

3. DEVICE STRUCTURE AND FABRICATION

The standard 894 nm epitaxial VCSEL structure grown on a (100) substrate is schematically illustrated in Fig. 2. The oxide-VCSEL consists of an active region with three $In_{0.1}Ga_{0.9}As/Al_{0.3}Ga_{0.7}As$ quantum wells. A top p-doped and bottom

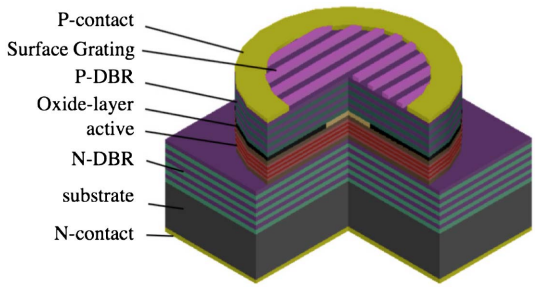

Fig. 2. Schematic view of surface grating VCSEL.

n-doped distributed Bragg reflector (DBR) of 22 and 34 $Al_{0.9}Ga_{0.1}As/Al_{0.12}Ga_{0.88}As$ mirror pairs are stacked on both sides of the quantum well gain region. A 30 nm thick $Al_{0.98}Ga_{0.02}As$ layer located above the p-type space layer is used to form the oxide aperture, which provides current and optical confinement. A 50 nm cap layer was on the top DBR. Thus, around 60 nm deep surface grating with a period of 600 nm is etched at the topmost GaAs layer. The duty cycle is 50%.

Here, we propose a two-step exposure technology to improve the surface grating fabrication on the top of VCSELs. First, large area grating lines were defined by DTL [22,23], which is a new mask-based photolithography technique for patterning high-resolution periodic patterns. The accuracy can also achieve the nanometer level as electron beam lithography, but it is low cost and time saving. The high-throughput lithography based on the Talbot effect takes advantage of monochromatic collimated light to illuminate a periodic structure, thus forming the self-images of the grating pattern at periodic intervals. By varying the gap between photolithography mask and the wafer corresponding to Talbot length, DTL is able to project periodic patterns easily without contaminating the original mask during the whole exposure procedure. However, the DTL lithography can be used only to form periodic structures. So the second exposure was carried out to reserve the grating lines within every circle mesa scale with a self-alignment process [25,26]. The process could be achieved by normal optical lithography, which required less resolution accuracy. This self-aligned process helps us to align the grating with respect to the mesa in the best possible way and make sure that there is a ridge of the grating in the center of the out-coupling facet. Thus, the simple technology is suitable for large-volume production. Figure 3 shows the patterns left in each step of the exposures.

Then, the grating was dry-etched using reactive ion etching (RIE). The mesa exposure was also made by a self-alignment technique, and sufficient depth was dry-etched to expose the high aluminum concentration layer by using the same RIE equipment as for the grating. The mesa was thereafter oxidized

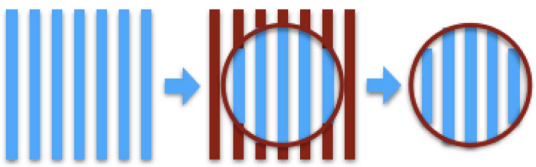

Fig. 3. Patterns left in each step of the exposures.

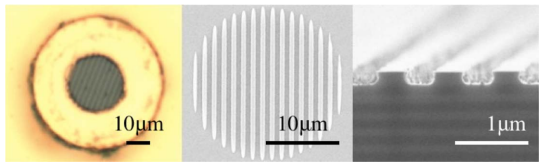

Fig. 4. Microscope image of a fully processed VCSEL (left) and SEM pictures of top and cross section of the grating (middle and right).

to form the oxide aperture with diameters of 3 μm and 5 μm to achieve single mode and multimode, respectively. Finally, the top p-contact (Ti/Pt/Au) and bottom n-contact (Au/Ge/Ni) were deposited and annealed by rapid thermal annealing at 400°C. Figure 4 shows a microscope image of fully processed VCSEL with a surface grating and scanning electron microscope pictures of the top and cross section of the grating.

4. EXPERIMENTAL RESULTS

VCSELs as compelling light sources for Cs-based atomic clocks need not only single polarization but also single mode under temperatures from 65°C to 80°C [25]. Therefore, the operation characteristics and polarization control under a high temperature of 80°C was measured mainly. Figure 5(a) depicts the polarization-resolved light-current (LI) characteristics of a surface grating VCSEL with an oxide aperture of 3 μm, a grating period of 600 nm, and a grating depth of 60 nm under a high temperature of 80°C and a room temperature of 20°C as a comparison. The optical powers of the two polarization directions are measured behind a Wollaston prism polarizer by orienting its transmission direction orthogonal and parallel to the grating lines. For the complete current range, the prior polarization orientation is strictly along the [0–11] crystal axis, which is orthogonal to the grating grooves under high temperature, as at room temperature. The sum of the measured powers in the two polarizations is lower than the total output power because of the losses in the Wollaston prism used in the measurement setup. The OPSR is calculated from the ratio of the two powers as

$$\mathrm{OPSR} = 10\log\left(\frac{P_{[0\text{–}11]}}{P_{[011]}}\right), \tag{2}$$

and is displayed in Fig. 5(a). The OPSR slightly decreases because of the decreased power of the device when the temperature increases. The average OPSR calculated from the data for currents in steps of 0.1 mA are all more than 19 dB at two temperatures. Moreover, the threshold current is 0.3 mA at 20°C and 0.5 mA at 80°C, respectively. It means that, though the grating was introduced on the top mirror of VCSEL, the threshold remains below 1 mA. Total output power at 1.5 mA is 0.55 mW under 20°C and 0.4 mW under 80°C, respectively.

The polarization-resolved high-temperature spectra were measured, and the results are shown in Fig. 5(b). The target wavelength of 894.6 nm is reached at a bias current of 1.5 mA with a side-mode suppression ratio of 35 dB. The difference between the dominant polarization peak and the suppressed polarization peak defined as peak-to-peak OPSR is approximately 30 dB, which exceeds the requirement of

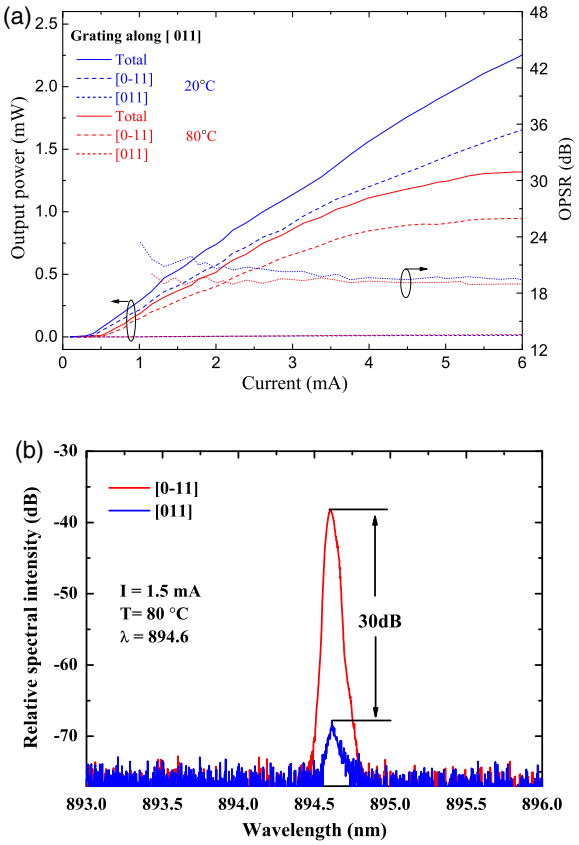

Fig. 5. Polarization-resolved LI characteristics: OPSR values (a) under a room temperature of 20°C and a high temperature of 80°C and polarization-resolved spectra (b) under a high temperature of 80°C of a grating VCSEL with an oxide aperture diameter of 3 μm. The grating period is 600 nm, and the grating depth is 60 nm.

classical atomic clocks of 20 dB. The OPSR taken from the spectra is larger than the calculated value from the LI characteristics because spontaneous emission is ignored in the peak-to-peak definition of the OPSR.

For an intuitive understanding of the beam quality of single-mode surface grating VCSEL, the emission far fields were measured at room temperature. Figure 6 shows the setup for measuring the far field of grating VCSEL by rotating the polarizer to make the polarization orientation of the polarizer orthogonal and parallel to the grating lines. Figure 7 shows the emission far fields of the single-mode grating VCSEL with two polarization orientations orthogonal and parallel to the grating lines. The beam performs a nearly perfect circular shape, and no emission side-lobes appear. The far-field angle = 8°. Therefore, the surface grating does not suffer from diffraction effects. The intensity of different polarizations verifies the polarization control capability of the surface grating VCSELs intuitively.

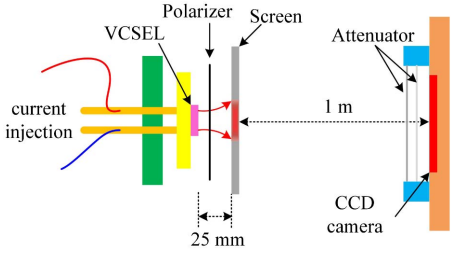

Fig. 6. Schematic diagram of experimental setup for measuring far field of single-mode grating VCSEL with two polarization orientations orthogonal and parallel to the grating lines.

Large-oxide aperture multi-mode VCSEL was measured as well. Figure 8 shows a grating VCSEL with an oxide diameter of 5 μm. The polarization-resolved light-current-voltage (LIV) characteristic and polarization-resolved spectra were measured. The threshold current is 0.2 mA. The average OPSR in the

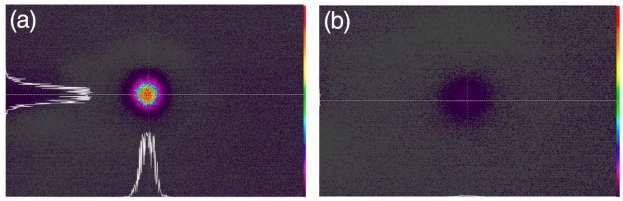

Fig. 7. Far fields of the single-mode polarization-stable VCSEL measured orthogonal (a) and parallel (b) to the grating lines at a bias of 1.5 mA under room temperature.

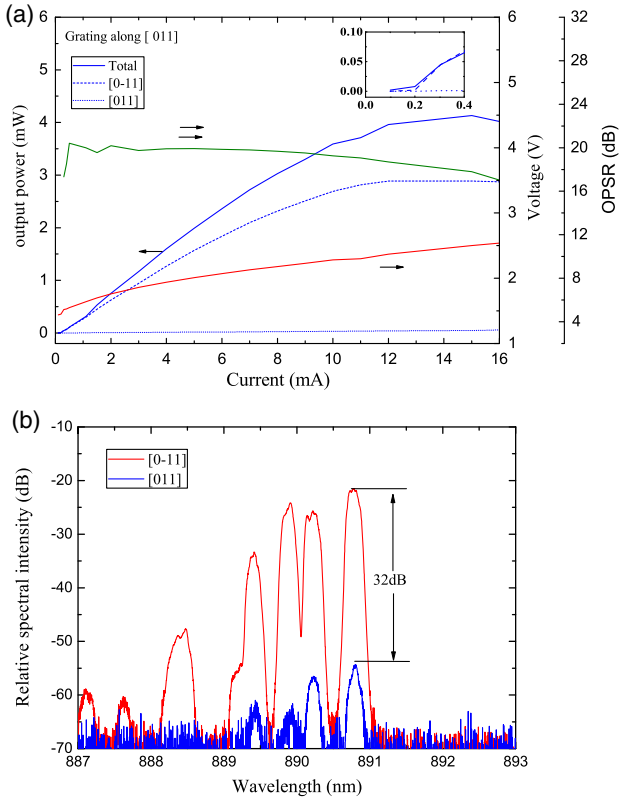

Fig. 8. Polarization-resolved LIV characteristics and OPSR values (a) and polarization-resolved spectra (b) measured under a temperature of 20°C of a grating VCSEL with an oxide aperture diameter of 5 μm. The grating period is 600 nm, and the grating depth is 60 nm.

Fig. 8(a) LIV graph is 19 dB, and the peak-to-peak OPSR is around 32 dB in Fig. 8(b).

5. CONCLUSION

The polarization control of single-mode 894 nm VCSELs integrated with shallow-surface gratings was achieved. The OPSR was 30 dB under 80°C. The threshold current is 0.5 mA at 80°C. Total output power at 1.5 mA is 0.4 mW at 80°C. The grating defined by taking advantage of the DTL was proposed. The improved grating VCSEL fabrication technology can easily be implemented into the existing process flow and be proved economically feasible for mass production. This type of grating VCSEL is promising for atomic clock applications. The multi-mode grating VCSEL was also measured. The OPSR was 32 dB.

Funding. National Key Research and Development Program (2017YFB0503200); National Natural Science Foundation of China (NSFC) (11674314, 11774343, 61434005, 61474118, 61727822); Science and Technology Program of Jilin Province, China (20160203013GX); Youth Innovation Promotion Association of the Chinese Academy of Sciences (2017260); Chinese Academy of Sciences President's International Fellowship Initiative (2018VTA0005).

REFERENCES

1. M. Shimizu, F. Koyama, and K. Iga, "Polarization characteristics of MOCVD grown GaAs/GaAlAs CBH surface emitting lasers," Jpn. J. Appl. Phys. **27**, 1774–1775 (1988).
2. M. P. Van Exter, V. D. A. K. Jansen, and J. P. Woerdman, "Electro-optic effect and birefringence in semiconductor vertical-cavity lasers," Phys. Rev. A **56**, 845–853 (1997).
3. M. Sanmigue, Q. Feng, and J. V. Moloney, "Light-polarization dynamics in surface-emitting semiconductor-lasers," Phys. Rev. A **52**, 1728–1739 (1995).
4. N. Nishiyama, A. Mizutani, N. Hatori, M. Arai, F. Koyama, and K. Iga, "Lasing characteristics of InGaAs-GaAs polarization controlled verticalcavity surface-emitting laser grown on GaAs [311] B substrate," IEEE J. Sel. Top. Quantum Electron. **5**, 530–536 (1999).
5. G. Verschaffelt, W. van der Vleuten, M. Creusen, E. Smalbrugge, T. G. van de Roer, F. Karouta, R. C. Strijbos, J. Danckaert, I. Veretennicoff, B. Ryvkin, H. Thienpont, and G. A. Acket, "Polarization stabilization in vertical-cavity surface-emitting lasers through asymmetric current injection," IEEE Photon. Technol. Lett. **12**, 945–947 (2000).
6. K. Panajotov, B. Nagler, G. Verschaffelt, A. Georgievski, H. Thienpont, J. Danckaert, and I. Veretennicoff, "Impact of in-plane anisotropic strain on the polarization behavior of vertical-cavity surface-emitting lasers," Appl. Phys. Lett. **77**, 1590–1592 (2000).
7. K. D. Choquette and R. E. Leibenguth, "Control of vertical-cavity laser polarization with anisotropic transverse cavity geometries," IEEE Photon. Technol. Lett. **6**, 40–42 (1994).
8. P. Debernardi, H. J. Unold, J. Maehnss, R. Michalzik, G. P. Bava, and K. J. Ebeling, "Single-mode, single-polarization VCSELs via elliptical surface etching: experiments and theory," IEEE J. Sel. Top. Quantum Electron. **9**, 1394–1404 (2003).
9. T. Mukaihara, N. Ohnoki, Y. Hayashi, N. Hatori, F. Koyama, and K. Iga, "Polarization control of vertical-cavity surface emitting lasers using a birefringent metal/dielectric polarizer loaded on top distributed Bragg reflector," IEEE J. Sel. Top. Quantum Electron. **1**, 667–673 (1995).
10. J. M. Ostermann, P. Debernardi, C. Jalics, and R. Michalzik, "Shallow surface gratings for high-power VCSELs with one preferred polarization for all modes," IEEE Photon. Technol. Lett. **17**, 1593–1595 (2005).
11. P. Debernardi, J. M. Ostermann, M. Feneberg, C. Jalics, and R. Michalzik, "Reliable polarization control of VCSELs through monolithically integrated surface gratings: a comparative theoretical and experimental study," IEEE J. Sel. Top. Quantum Electron. **11**, 107–116 (2005).
12. M. J. Miah, A. Al-Samaneh, A. Kern, D. Wahl, P. Debernardi, and R. Michalzik, "Fabrication and characterization of low-threshold polarization-stable VCSELs for Cs-based miniaturized atomic clocks," IEEE J. Sel. Top. Quantum Electron. **19**, 1701410 (2013).
13. P. Debernardi and G. P. Bava, "Coupled mode theory: a powerful tool for analyzing complex VCSELs and designing advanced device features," IEEE J. Sel. Top. Quantum Electron. **9**, 905–917 (2003).
14. A. Al-Samaneh, M. T. Haidar, D. Wahl, and R. Michalzik, "Polarizationstable single-mode VCSELs for Cs-based miniature atomic clocks," in *Conference on Lasers and Electro-Optics Europe and 12th European Quantum Electronics Conference (CLEO EUROPE/EQEC)* (IEEE, 2011), p. 1.
15. M. C. Y. Huang, Y. Zhou, and C. J. Chang-Hasnain, "A surface-emitting laser incorporating a high-index-contrast subwavelength grating," Nat. Photonics **1**, 119–122 (2007).
16. C. J. Chang-Hasnain and W. Yang, "High-contrast gratings for integrated optoelectronics," Adv. Opt. Photon. **4**, 379–440 (2012).
17. P. Qiao, K. Li, K. T. Cook, and C. J. Chang-Hasnain, "MEMS-tunable VCSELs using 2D high-contrast gratings," Opt. Lett. **42**, 823–826 (2017).
18. M. C. Y. Huang, Y. Zhou, and C. J. Chang-Hasnain, "Polarization mode control in high contrast subwavelength grating VCSEL," in *Conference on Lasers and Electro-Optics* (IEEE, 2008), pp. 1–2.
19. Y. Yang, G. Djogo, M. Haque, P. R. Herman, and J. K. S. Poon, "Integration of an O-band VCSEL on silicon photonics with polarization maintenance and waveguide coupling," Opt. Express **25**, 5758–5771 (2017).
20. M. A. Verschuuren, P. Gerlach, H. A. van Sprang, and A. Polman, "Improved performance of polarization-stable VCSELs by monolithic sub-wavelength gratings produced by soft nano-imprint lithography," Nanotechnology **22**, 505201 (2011).
21. M. Grabherr, R. King, R. Jäger, D. Wiedenmann, P. Gerlach, D. Duckeck, and C. Wimmer, "Volume production of polarization controlled single-mode VCSELs," Proc. SPIE **6908**, 690803 (2008).
22. H. Chen, L. Qin, Y. Chen, P. Jia, F. Gao, C. Chen, L. Liang, X. Zhang, H. Lou, Y. Ning, and L. Wang, "Refined grating fabrication using displacement Talbot lithography," Microelectron. Eng. **189**, 74–77 (2018).
23. H. H. Solak, C. Dais, and F. Clube, "Displacement Talbot lithography: a new method for high-resolution patterning of large areas," Opt. Express **19**, 10686–10691 (2011).
24. C. W. Haggans and L. Li, "Convergence of the coupled-wave method for metallic Lamellar diffraction gratings," J. Opt. Soc. Am. A **10**, 2217–2225 (1993).
25. A. Al-Samaneh, M. Bou Sanayeh, S. Renz, D. Wahl, and R. Michalzik, "Polarization control and dynamic properties of VCSELs for MEMS atomic clock applications," IEEE Photon. Technol. Lett. **23**, 1049–1051 (2011).
26. L. Marigo-Lombart, A. Arnoult, L. Mazenq, P. Dubreuil, B. Reig, N. Mauran, H. Thienpont, K. Panajotov, and G. Almuneau, "Single lithography-step self-aligned fabrication process for vertical-cavity surface-emitting lasers," Mater. Sci. Semicond. Process. **61**, 35–38 (2017).